Evaluating the Potential and Added Value of Interferometric Coherence in Flood Mapping Across Various Environments

Sulaiman Fayez Hotaki[1], Mahmud Haghshenas Haghighi[1], Mahdi Motagh[1,2]

[1]Institute of Photogrammetry and GeoInformation, Leibniz University Hannover,
Hannover 30167, Germany (hotaki@ipi.uni-hannover.de)
[2]GFZ German Research Centre for Geosciences, Department of Geodesy, Section of Remote Sensing,
Potsdam 14473, Germany (mahdi.motagh@gfz.de)

Keywords: Flood mapping, SAR, Interferometric Coherence, Remote sensing, Sentinel-1.

Abstract

Flood mapping is one of the most important applications of Synthetic Aperture Radar (SAR) because it can monitor the earth's surface under all-weather, day-and-night conditions. While SAR intensity has been widely used for flood mapping, the potential and added value of interferometric coherence, especially its temporal behavior in different environments, remains mostly unexplored. In this study, we assess the potential and added value of interferometric coherence from Sentinel-1 time series for flood mapping in three contrasting regions: the urban area of Valencia (Spain), the arid region of Sistan and Baluchestan (Iran), and the agricultural area of Hannover (Germany). Our analysis of multi-temporal coherence shows that coherence provides clear flood indicators in arid regions through strong temporal decorrelation, but its performance is less reliable in vegetated and urban areas. In agricultural regions, pre-flood (baseline) coherence is inherently low due to vegetation phenology and temporal decorrelation, making any additional decrease due to flood inundation often indistinguishable. In urban areas, coherence generally remains stable, with only slight decreases observed in specific cases; therefore, the detectability of flooded areas using coherence-based approaches is limited in both agricultural and urban environments. In contrast, coherence in arid regions is high before flooding and drops significantly during flood events, making floods easy to detect in such regions. These findings demonstrate that, for flood mapping, interferometric coherence is a valuable but environment-dependent indicator, with the highest benefit seen in arid regions where intensity-based methods are limited.

1. Introduction

Flooding is one of the most widespread natural disasters worldwide, causing severe socio-economic and environmental impacts. Accurate and timely flood mapping is crucial for disaster management, emergency response, and mitigation planning. Remote sensing technologies, particularly Synthetic Aperture Radar (SAR), play a vital role in flood mapping because of their ability to acquire imagery regardless of weather conditions or daylight availability (Pulvirenti et al., 2011; Sharifi, 2020; Chini et al., 2021; Amitrano et al., 2024). In contrast to optical remote sensing, which is often limited by clouds, SAR sensors are enable to penetrate the clouds during flood events (Townsend, 2001).

SAR intensity-based flood mapping is widely recognized as a reliable and state-of-the-art approach, forming the backbone of most operational flood mapping methods due to its sensitivity to changes in surface water conditions (Nico et al., 2000; Pandey et al., 2022; Vanama et al., 2020; Anusha and Bharathi, 2020). Water bodies typically appear as areas of low backscatter in SAR Intensity images because smooth water surfaces cause specular reflection (Oberstadler et al., 1997; Nico et al., 2000).

However, Intensity-based approaches face challenges in complex environments, for example, urban areas, where double-bounce backscattering from man-made structures is dominant (Delgado Blasco et al., 2020; Liao and Wen, 2020). Similarly, arid and bare soil regions, due to their dry, smooth surfaces, also reflect SAR signals like surface water, leading to low backscatter and further complicating reliable flood detection when using intensity data alone (Martinis, 2017; Garg et al., 2024). An alternative for Intensity-based flood mapping is the interferometric coherence, which is one of the main InSAR (Interferometric Synthetic Aperture Radar) products, that describes the correlation coefficient between two SAR images acquired at different times (Zebker et al., 1992; Nico et al., 2000; Zhang et al., 2021). A few studies have explored its potential for flood mapping. For instance, (Li et al., 2019) employed a Bayesian-network fusion of SAR intensity and coherence for urban flood mapping, which showed robust performance when validated with high-resolution imagery. Similarly, (Papila et al., 2020; Soudagar and Bhardwaj, 2025) integrated intensity and coherence change detection for urban and agricultural flood mapping using Sentinel-1 data, utilizing a region growing technique with a seed that was chosen using high-resolution optical imagery. In their work, Soudagar and Bhardwaj (2025) integrated SAR intensity and coherence for flood mapping by applying a Gaussian Mixture Model to segment both intensity change derived using normalized change index (NCI) and coherence difference, and then fused these classified results using logical operations to delineate flooded urban and bare soil areas. In another study, (Garg et al., 2024) combined coherence and amplitude features in a Random Forest classifier to map arid-region floods using a limited number of Sentinel-1 pairs.

Despite these developments, in comparison to the SAR Intensity, interferometric coherence remains underutilized for flood mapping. Most studies have focused on a single pre-flood and post-flood image pair or by combining coherence with Intensity data. The potential and added value of Interferometric coherence and time series behavior of coherence for flood mapping remained unexplored. This study addresses this gap

This contribution has been peer-reviewed. The double-blind peer-review was conducted on the basis of the full paper.
https://doi.org/10.5194/isprs-annals-XI-3-2026-419-2026 | © Author(s) 2026. CC BY 4.0 License.

by analyzing Interferometric coherence in multiple flood regions. Unlike comparative intensity and coherence studies, we specifically evaluate coherence's standalone potential and environment-dependent added value, using intensity only as a baseline benchmark. We analyze the potential of interferometric coherence for studying floods across three distinct environments, such as Spain, Germany, and Iran. Our main focus relies on the potential and added value of interferometric coherence for flood mapping, while intensity-based flood mapping is used as a baseline method and benchmark.

2. Methodology

This study evaluates the added value and potential of coherence for flood mapping using multi-temporal Sentinel-1 data across diverse environments. While intensity is widely established for flood detection, it is used here as a reference or baseline; our analysis centers on the performance and contribution of interferometric coherence for flood mapping. The methodology consists of three steps, as shown in Figure 1.

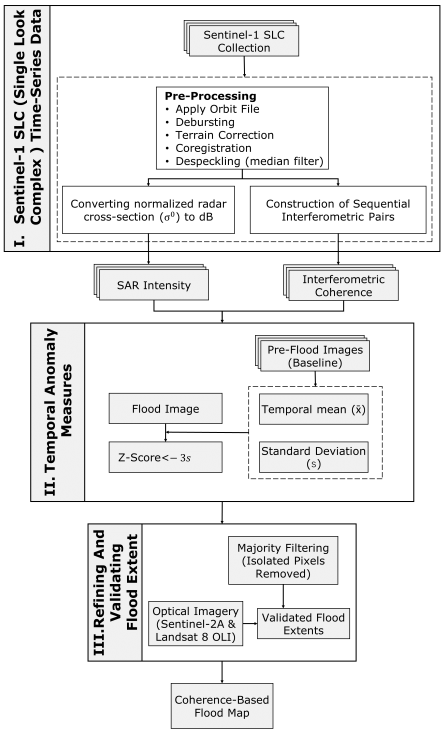

Figure 1. Overview of the processing workflow used to assess the potential and added value of interferometric coherence for flood mapping.

First, Sentinel-1 SAR images covering each study period were co-registered into a single SLC stack using the GAMMA software. From this SLC stack, backscatter intensity was computed, followed by application of a median filter with a 3×3 window to reduce speckle noise.

The resulting intensities are expressed as normalized radar cross-section (σ^0) values in decibels (dB) according to (Richards et al., 2009)

$$\sigma^0_{(\mathrm{dB})} = 10 \log_{10} \sigma^0 \tag{1}$$

The interferometric coherence, defined as the normalized correlation coefficient between the two SAR images (Zebker et al., 1992), was calculated as follows:

$$\rho = \frac{|\langle s_1 s_2^* \rangle|}{\sqrt{(\langle s_1 s_1^* \rangle \langle s_2 s_2^* \rangle)}} \tag{2}$$

Here, s_1 and s_2 represent complex-valued pixels of two SAR images, the * denotes complex conjugation, and the angle brackets in Eq. 2 indicate statistical expectation, typically obtained by spatial averaging with a boxcar filter (Rosen et al., 1996; Ferretti et al., 2011). To further reduce speckle and improve the signal-to-noise ratio (SNR) of the coherence estimates, we applied multi-looking with a window size of 10×2 in azimuth and range, respectively. A coherence value near 1 corresponds to no changes, while surface changes cause decorrelation and lower the value of coherence (ρ). Interferometric Coherence in repeat-pass interferometry is influenced by three main factors (Zebker et al., 1992).

$$\rho = \rho_N \cdot \rho_S \cdot \rho_T \tag{3}$$

The correlation of the thermal noise is represented by ρ_N, the spatial correlation by ρ_S, and the temporal correlation by ρ_T. We are interested in ρ_T and how it is impacted by the flood. Therefore, we need to isolate the other two terms. The observation system and electronic components are the source of thermal noise, which reduces correlation in the case of Sentinel-1 is typically negligible (Fielding and Jung, 2024; Lu et al., 2018). The perpendicular baseline, on the other hand, regulates spatial baseline decorrelation (Lu et al., 2018; Ishitsuka et al., 2012). Smaller perpendicular baselines preserve coherence. Sentinel-1 is designed to maintain a narrow orbital tube with perpendicular baselines, typically within ± 150 meters to minimize the effect of ρ_S. Temporal correlation ρ_T may be impacted by environmental changes other than floods, such as seasonal or land cover changes. To minimize the impact of seasonal changes and the effect of land cover variation on the coherence, shorter temporal baselines are preferred. Thus, we kept a temporal baseline of 12 days for estimating the Interferometric coherence.

Secondly, for each flood event and study area, a set of pre-flood images was used to compute the pixel-wise pre-flood mean for both intensity and coherence. A single pre-flood image was also selected. These were compared with a flood image acquired during the event, enabling assessment of the interferometric coherence's response to flooding.

Flood extents were derived using temporal anomaly measures from both intensity and coherence. For each pixel, a baseline is formed using approximately one year of pre-flood Sentinel-1 SLC data, from which the temporal mean ($\bar{x}_i$) and standard deviation (s) are calculated. To detect flood extent, we used a per-pixel standardized score (Z) that was calculated as:

$$Z = \frac{x_i - \bar{x}_i}{s} \tag{4}$$

In this approach, x_i is the value of pixel *i*, while $\bar{x}_i$ and s are the temporal mean and standard deviation for that pixel from the pre-flood baseline. For each pixel, we calculate how much its value during the flood differs from its usual (baseline) value. If the change is greater than a certain number of standard deviations from the normal, we mark it as an anomaly, meaning it is likely flooded or affected by the flood. The value you choose for this threshold can be adjusted based on confidence level; for example, setting it to $Z < -3$, means only a very small number of pixels, less than 0.13% would be marked as flood by chance (Frost, 2019), so we can be quite confident that the detected anomalies really are related to flooding. A majority filter was applied to refine the flood extent, retaining a pixel as

flooded only if at least eight of its neighbors were also classified as flooded.

Finally, coherence-based flood extents converted from radar coordinates to geographical coordinates and validated against available optical satellite imagery, specifically Sentinel-2A (14 January 2020) for Sistan and Baluchestan, Iran, and Landsat 8 OLI (Operational Land Imager) (31 October 2024) for Valencia, Spain. Validation was performed using 500 randomly sampled points in each study area, selected by a random sampling method to ensure unbiased accuracy assessment (Stehman, 1999). No suitable optical dataset was available for Hannover, Germany, so validation could not be performed for this site. The agreement between coherence-based flood extents and optical reference data was quantitatively assessed using confusion matrices.

2.1 Study Area

This study focuses on three different regions that represent varying environmental conditions: the urban environment of Valencia, Spain; the arid region of Sistan and Baluchestan, Iran; and the agricultural and urban region of Hannover, Germany.

The Valencia region, in eastern Spain, spans 23,255km^2 and includes the provinces of Castellon, Valencia, and Alicante. Most areas experience an arid to semi-arid climate, with sub-humid conditions near the Mediterranean coast. This study focuses on the Valencia Metropolitan Area, a densely populated coastal zone, severely impacted by flooding after intense storms in October 2024.

The second site is Sistan and Baluchestan, Iran’s second-largest province (180,726km^2, population about 2.5 million), is located in the southeast bordering Pakistan and Afghanistan. The province is mostly desert with very high temperatures and minimal rainfall. However, severe flooding occurred following intense rainfall between January 8-13, 2020.

The third study area, Hannover in central Lower Saxony, features both agricultural land and urban areas, and lies within the catchments of the Ems, Weser, and Elbe rivers. Heavy rainfall throughout December 2023 and January 2024 led to widespread flooding in this region.

2.2 Dataset

Sentinel-1 SLC (Single Look Complex) in interferometric wide-swath (IW) mode is used in this study. Both intensity and interferometric coherence images were derived from the SLC time series acquired before, during, and after flood events at each study area. Interferometric coherence was calculated sequentially from pairs of co-registered SLC images. Details of the Sentinel-1 SLC datasets used for the three study areas are given in Table 1.

As shown in Table 1, VV polarization was selected for all study areas, as it provides superior sensitivity to floodwater detection and stronger contrast between water and non-water surfaces compared to VH polarization, which is more influenced by volume scattering from vegetation and complex surfaces (Twele et al., 2016).

Study Area	Date Range	Images	Polarization	Orbit
Valencia, Spain	2023-10-01 to 2024-10-31	34	VV	Ascending
Sistan and Baluchestan, Iran	2019-01-09 to 2020-01-16	31	VV	Descending
Hannover, Germany	2023-01-01 to 2023-12-27	31	VV	Descending

Table 1. Overview of Sentinel-1 SLC data characteristics for each study area.

3. Results

The findings from Sentinel-1 data in three different regions are shown in this section. SAR intensity and interferometric coherence were used in the analysis, and the results are presented separately for each study area.

3.1 Valencia, Spain

The flood occurred in Valencia on 31 October 2024. Valencia city consists of both urban and agricultural areas, but our analysis mainly focused on the urban regions, particularly around Xirivella, La Torre, and the Turia river, which were affected by flooding. As shown in Figure 2 (A, B, and C), intensity values remained high across the 1-year pre-flood mean, the pre-flood image, and the flood image. The pre-flood mean intensity image (Figure 2, A) appears less noisy, which is reflected in its histogram where most values cluster around the mean intensity (mean = -29dB) with a small standard deviation (std = 4.2dB), as shown in Figure 3. The pre-flood intensity image looks visually similar to the pre-flood mean intensity image, but it is noticeably noisier. This is evident from its histogram (see Figure 3), with a mean of -30dB and a higher standard deviation (std = 5dB). In contrast, the flood intensity image (Figure 2, C) displays clear signs of flooding along the Turia River and in the bottom-right of the flood image, typically corresponding to agricultural lands near Lake L’Albufera. The flood intensity image has nearly the same mean (-29dB) and a slightly higher standard deviation (std = 5.3 dB) than the pre-flood images. However, no major low-intensity values are observed within the city itself. Overall, the intensity values have not changed significantly compared to the pre-flood intensity and pre-flood mean intensity images.

Meanwhile, as shown in Figure 2 (D, E, and F), coherence is generally high in urban areas and low in agricultural areas. The pre-flood mean coherence image (Figure 2, D) appears less noisy, with a mean value of 0.6 and a standard deviation of 0.2. The minimum and maximum coherence values in this image range from 0.23 to 1. In contrast, the pre-flood coherence image (Figure 2, E) is noisy, with values ranging from 0 to 0.9, a mean of 0.5, and a standard deviation of 0.25 as shown in 3. In the flood coherence image, some low coherence values are observed in the Turia river, Xirivella, and La Torre areas, as well as in the bottom-right part of the image, compared to the pre-flood coherence image, as shown in (Figure 2, F). The mean and standard deviation for the flood coherence image are 0.5 and 0.25, respectively. Since this region includes a mix of urban and agricultural areas, the pre-flood mean coherence shows the distinct peaks, one around 0.4 and one around 0.8, corresponding to urban and non-urban areas, as shown in Figure 3. While the histogram of the pre-flood coherence image skewed to the right, it might be affected by noise and temporary decorrelation

sources like vegetations, but for most urban or bare areas, it remains high. The flood coherence image is skewed to the left; this shape reflects dramatic decorrelation caused by flooding.

The flood extent maps derived from temporal anomaly measures for Valencia, shown in Figure 4, highlight some interesting differences between the intensity-based and coherence-based methods. The intensity map mainly captures flooding along the Turia River and in agricultural areas. In contrast, the coherence map detected flooding along the Turia River and scattered patterns, mostly in urban areas, where intensity changes are not strong.

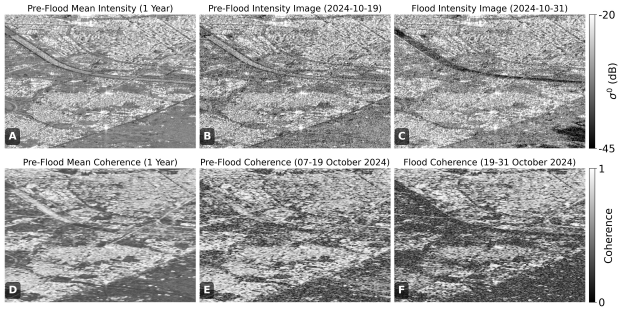

Figure 2. Sentinel-1 SAR intensity (top row) and interferometric coherence (bottom row) images illustrating flood-affected areas in Valencia, Spain. Panels (A-C) show the pre-flood mean, pre-flood, and flood intensity images, respectively. Panels (D-F) present the corresponding coherence images before and during the flood event (October 2024). Flooded areas appear darker in intensity images and exhibit reduced coherence values, particularly along the Turia River and surrounding urban regions.

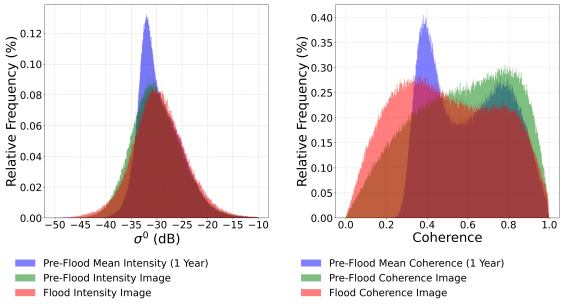

Figure 3. Histograms of pre-flood mean, pre-flood, and flood intensity (left) and coherence (right) images for the Valencia, Spain flood event in October 2024. The left panel shows the distribution of radar backscatter intensity values in dB, while the right panel presents the distribution of coherence values. In the flood maps, the intensity histogram shifts slightly toward lower values for pre-flood and flood images, indicating reduced backscatter from flooded surfaces. The coherence histogram shifts toward lower values during the flood, with the pre-flood mean coherence showing two peaks that indicate the existence of urban and agricultural areas.

3.2 Sistan and Baluchestan

In the Sistan and Baluchestan province of Iran, which is generally an arid region, a flood occurred on 13 January 2020. Overall, all three intensity images appear dark due to the naturally low backscatter values in this arid region as shown in (Figure 5, A, B, and C). However, some bright areas with higher intensity can be seen, which correspond to man-made infrastructures and

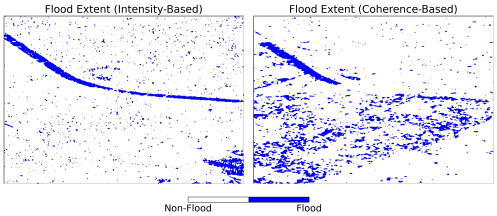

Figure 4. Flood extents for Valencia, Spain, derived from intensity-based (left) and coherence-based (right) using temporal anomaly measures.

mountain ranges. The pre-flood mean intensity image (Figure 5, A) has a mean value of (mean=-39dB) and a standard deviation of (Std=4.3dB), appearing less noisy, with most pixel values concentrated around the mean, as shown in Figure 6. Similarly, the pre-flood intensity image (Figure 5, B) dated 04 January 2020 also shows very low intensity values, with a mean of -39dB and a standard deviation of 5.8dB. Although it appears slightly noisier, it looks visually similar to the pre-flood mean intensity image. The flood intensity image (Figure 5, C) taken on 16 January 2020, in general, also appears dark like the pre-flood images. However, as shown in Figure 6, a small decrease in pixel values is observed around -50dB, likely associated with flooding, but overall, no significant and distinct changes can be measured. Several darker patches can be observed in the bottom-left part of the image (see Figure 5, C), which likely represent flooded areas. The mean intensity slightly decreases to -41 dB, and the standard deviation increases to 6.5dB compared to the pre-flood mean intensity and pre-flood intensity images. Overall, all three intensity images already have very low intensity values, making it difficult to clearly distinguish between flooded and non-flooded areas.

Unlike the intensity images, the pre-flood mean coherence image (Figure 5, D) in Sistan appears bright, with a mean of 0.6 and a very small standard deviation of 0.1, indicating minimal noise (see Figure 6). The pre-flood coherence image is even brighter, with a mean of 0.7 and a standard deviation of 0.19, suggesting no significant surface changes before the flood as shown in (Figure 5, E). In contrast, the coherence values drop significantly in the flood coherence image (Figure 5, F), with a mean of 0.35 and a standard deviation of 0.22. As shown in Figure 6, the pre-flood coherence values are centered around 0.7, whereas in the flood coherence image, most values are around 0.3. In the pre-flood mean coherence image, the majority of values cluster near 0.6.

The flood extent maps derived from temporal anomaly measures of intensity and coherence (see Figure 7) show the impact of each approach. The intensity-based flood extent detects floods only in some limited patches across the intensity image, while the coherence-based flood extent captures a much broader and more continuous floodplain. This indicates that coherence is more sensitive to flooding in this environment.

3.3 Hannover, Germany

A flood occurred in Hannover, Germany, on 27 December 2023. Hannover city consists of both agricultural and urban areas. The flood mainly affected the agricultural lands, as shown in (Figure 8, A, B, and C). In the pre-flood mean intensity image (Figure 8, A), no significant changes are observed; however, the agricultural areas appear slightly darker than their surroundings. The pre-flood mean intensity image appears less noisy, with a mean

This contribution has been peer-reviewed. The double-blind peer-review was conducted on the basis of the full paper.
https://doi.org/10.5194/isprs-annals-XI-3-2026-419-2026 | © Author(s) 2026. CC BY 4.0 License.

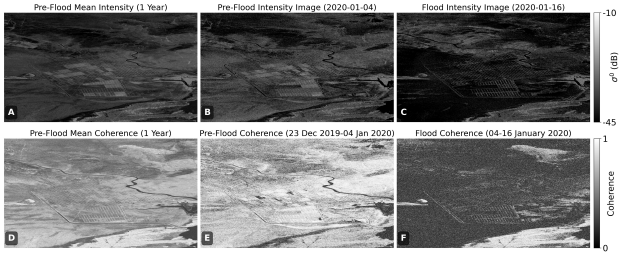

Figure 5. Sentinel-1 SAR intensity (top row) and coherence (bottom row) images for the Sistan and Baluchestan, Iran flood event (January 2020). Panels (A-C) show pre-flood mean, pre-flood, and flood intensity images, while (D-F) present corresponding coherence images. Both non-flood and flood areas appear darker in intensity images. while coherence dropped only in the flood coherence image.

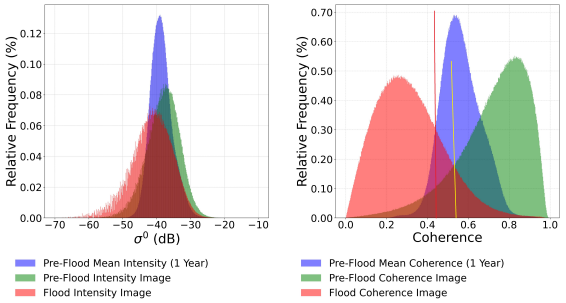

Figure 6. Histograms of pre-flood mean, pre-flood, and flood intensity (left) and coherence (right) images for the Sistan and Baluchestan flood event (January 2020). The intensity histogram shifts toward lower values during flooding, while coherence drops sharply during the event. The red and yellow vertical lines on the coherence histogram are only for visual guidance, to show that flood and non-flood areas can be distinguished in the histogram.

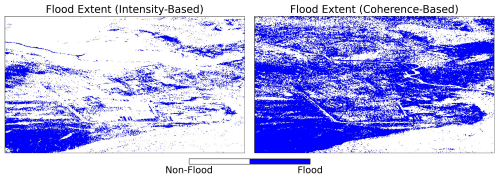

Figure 7. Flood extent map for Sistan and Baluchistan, Iran, derived from temporal anomaly measures: (left) intensity-based and (right) coherence-based results.

of -31dB and a standard deviation of 2.7dB, as shown in Figure 9. In the pre-flood intensity image (Figure 8, B) acquired on 15 December 2023, several low-intensity spots can be observed in the agricultural lands, possibly caused by rainfall or irrigation, but no notable changes have occurred. The pre-flood intensity image is noisier than the pre-flood mean intensity image, with a mean of -30dB and a standard deviation of 4dB. In contrast, the flood intensity image clearly shows dark pixels or low-intensity areas in the agricultural lands, as illustrated in (Figure 8, C). The mean intensity decreases to -33dB, and the standard deviation increases significantly to 5.5dB. The flood intensity histogram shows the appearance of some low values near -40dB compared to the pre-flood images due to the flood, as shown in Figure 9.

While the flooded areas appear much darker and can be visually distinguished from non-flooded regions in the intensity images, the coherence images display a different pattern. Coherence remains consistently low in agricultural and green areas but high in urban zones across all images, as shown in (Figure 8, D, E, and F). The pre-flood mean coherence image is relatively less noisy, with a mean of 0.4 and a standard deviation of 0.18. The pre-flood coherence image appears noisier but maintains similar statistical values, with a mean of 0.4 and a standard deviation of 0.2. Interestingly, in the flood coherence image, agricultural areas continue to show low coherence values, while some other areas that previously showed low coherence exhibit higher coherence values. The mean value of the flood coherence image is 0.44, with a standard deviation of 0.22. As seen in Figure 9, the histograms of the three coherence images in the right panel show no significant change, with most values clustering around 0.4. Therefore, it is difficult to distinguish between flooded and non-flooded areas based on coherence, as agricultural lands consistently exhibit low coherence values.

The different patterns detected by intensity-based and coherence-based based are also reflected in the flood extent maps for Hannover, as shown in Figure 10. The intensity-based map (left) highlights clear flooded areas mainly along the river and in certain agricultural fields, which appear as distinct, connected patches. The coherence-based map (right), however, detects far fewer flooded pixels, and they are distributed more sparsely, often as small, isolated spots instead of large, continuous regions. This suggests that coherence in Hannover was less sensitive to the changes caused by flooding, especially in the wide agricultural areas.

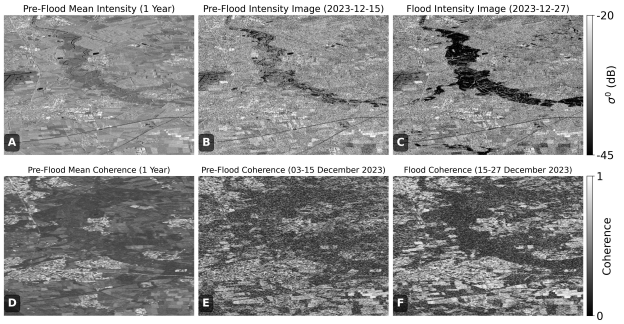

Figure 8. Sentinel-1 SAR intensity (top row) and interferometric coherence (bottom row) images showing flood-affected areas in Hannover, Germany. Panels (A-C) display the pre-flood mean, pre-flood, and flood intensity images, respectively; panels (D-F) show the corresponding coherence images before and during the December 2023 flood event. Flooded areas appear darker in the flood intensity image, particularly over agricultural fields, while coherence remains consistently low across the agricultural areas, regardless of flooding, due to rapid vegetation and surface changes.

3.4 Accuracy Assessment

To quantitatively assess the performance of coherence-based flood mapping while intensity-based maps are used as reference and not included in the validation process, validation was conducted by selecting 500 random points in the study areas with available reference data and comparing coherence-based flood maps to reference satellite imagery. We validated using Sentinel-2 and Landsat 8 imagery, which are standard for flood detection, but their resolutions match Sentinel-1’s, which may underestimate our SAR accuracy. Clouds also often pre-

This contribution has been peer-reviewed. The double-blind peer-review was conducted on the basis of the full paper.
https://doi.org/10.5194/isprs-annals-XI-3-2026-419-2026 | © Author(s) 2026. CC BY 4.0 License.

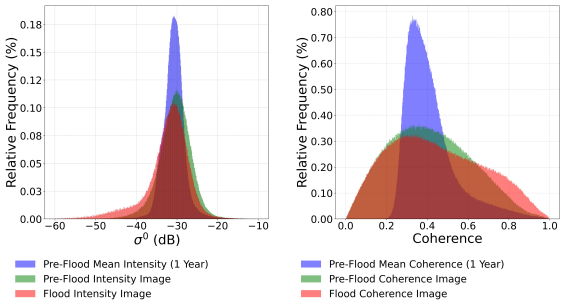

Figure 9. Histograms of pre-flood mean, pre-flood, and flood intensity (left) and coherence (right) images for the Hannover, Germany flood event in December 2023. The left panel shows intensity distributions, slightly shifted to lower values in the flood image. The coherence histogram in the right panel remains nearly unchanged between pre-flood and flood, with the pre-flood mean histogram sharply peaked near 0.4, indicating low noise and stable surface conditions.

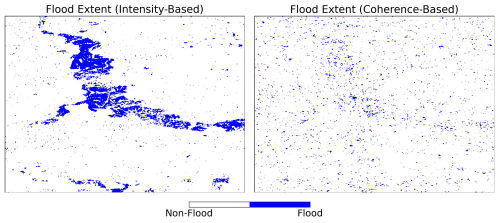

Figure 10. Flood extent map for Hannover, Germany, derived from temporal anomaly measures: (left) intensity-based and (right) coherence-based results.

vent timely optical data during floods. Hence, for the Hannover region, suitable reference imagery was unavailable, so validation could not be performed for this site. Therefore, only two study areas were validated. In Valencia, a confusion matrix was calculated using Landsat 8 OLI optical data as reference (Figure 11), and key accuracy metrics are summarized in Table 2. Coherence-based flood mapping achieved high precision (0.87), so detected floods usually correspond to true inundation. Recall, however, was low (0.16), indicating that most actual flooded pixels were missed. Specificity was excellent (0.97), showing reliable identification of non-flooded areas. Overall accuracy was moderate (0.58), with a low F1 score (0.28), reflecting an imbalance between precision and recall.

Study Areas	Precision	Recall	Specificity	Accuracy	F1
Valencia	0.87	0.16	0.97	0.58	0.28
Sistan	0.70	0.78	0.47	0.65	0.73

Table 2. Performance metrics for Coherence-based flood detection in each study area.

In Sistan, coherence-based flood detection was evaluated using Sentinel-2A optical data as reference (Figure 12), with results summarized in Table 2. The results show moderately high precision (0.70) and high recall (0.78), indicating strong sensitivity to flooded pixels. Specificity (0.47) was lower, with some overmapping of non-flooded areas, but overall accuracy (0.65) and F1 score (0.73) demonstrate a good balance between precision and recall.

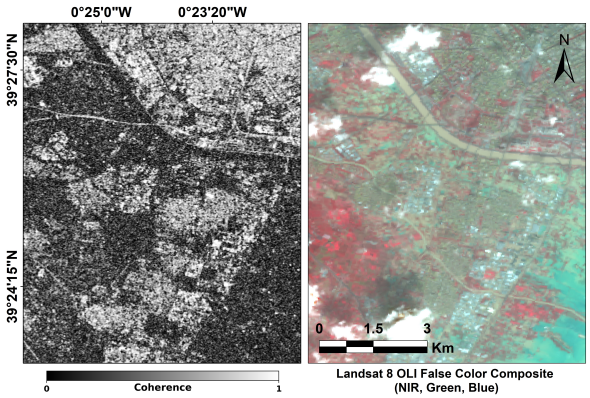

Figure 11. Sentinel-1 geocoded coherence map (left) and Landsat 8 OLI false color composite (NIR, Green, Blue; right) for urban areas in Valencia, Spain. The optical image serves as a reference for validating coherence-based flood extent, with accuracy metrics reported in Table 2. In the false color composite, muddy and greenish areas indicate flooding and surface water, red areas indicate vegetation, and bright areas depict urban areas.

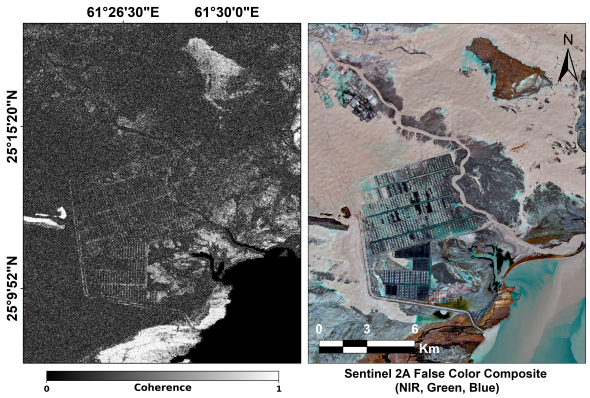

Figure 12. Sentinel-1 geocoded coherence map (left) and Sentinel-2A false color composite (NIR, Green, Blue; right) for the arid regions in Sistan and Baluchistan, Iran. The optical image serves as a reference for validating the coherence-based flood extent, with accuracy metrics reported in Table 2. Areas of low coherence mark flooded zones. In the false color image, muddy areas indicate flooding, and greenish regions correspond to surface water.

4. Discussion

This study evaluated the potential and added value of interferometric coherence for flood mapping in three different environments: urban (Valencia, Spain), arid (Sistan and Baluchestan, Iran), and agricultural (Hannover, Germany), using Sentinel-1 SAR time series data.

Coherence values in low-coherence regions tend to be biased and systematically higher than their true values due to spatial averaging (Touzi et al., 2002), which can limit their reliability for flood detection. To reduce these effects, a multi-looking window of 10x2 pixels (range × azimuth) was selected as a balance between speckle reduction and spatial resolution, following established practices in SAR coherence estimation (Touzi et al., 2002; Bickel, 2014). Other window sizes, such as 5×2 or 10×20, were tested but found to either leave excessive speckle or reduce image resolution.

This contribution has been peer-reviewed. The double-blind peer-review was conducted on the basis of the full paper.
https://doi.org/10.5194/isprs-annals-XI-3-2026-419-2026 | © Author(s) 2026. CC BY 4.0 License.

A temporal baseline using multiple pre-flood images was used to provide a stable reference for detecting flood-induced changes. Averaging across several pre-flood acquisitions reduces speckle and short-term surface variability, leading to more reliable flood detection (Vanama et al., 2020). Flood pixels were identified using a z-score threshold of $Z < -3$, which represents a high confidence level with fewer than 0.13% false positives under normal conditions (Frost, 2019). Adjusting the threshold (for example, to -2.5 or -2) can improve sensitivity in certain conditions, as discussed by (DeVries et al., 2020).

The following sections discuss the performance of interferometric coherence and intensity for flood mapping in each environment.

4.1 Urban Environment (Valencia)

In Valencia, radar intensity remained generally high and stable within urban areas, with noticeable reductions along the Turia River and the agricultural land near Lake L'Albufera. Only the VV polarization was used because it provides better sensitivity to floodwater and stronger contrast between water and non-water surfaces compared to VH polarization (Twele et al., 2016). However, strong backscatter from urban surfaces due to double-bounce scattering limited the ability of intensity data to detect floods, a problem also noted by (Delgado Blasco et al., 2020; Liao and Wen, 2020). A slight decrease in coherence was observed around Xirivella, La Torre, and along the Turia River, but overall, neither coherence nor intensity could reliably detect floods in the urban area. The medium spatial resolution of Sentinel-1 and the averaging during coherence estimation (boxcar) further reduced the ability to identify small-scale flooding.

4.2 Arid Environment (Sistan and Baluchestan)

In the arid region of Sistan and Baluchestan, intensity-based flood mapping was ineffective because the dry, sandy surface already produced low backscatter similar to open water. This made it difficult to distinguish flooded from non-flooded areas using intensity alone.

In contrast, interferometric coherence clearly identified flooded regions. Coherence values dropped sharply during the flood event but remained high in pre-flood images, providing a strong separation between flooded and unaffected areas. These results agree with previous studies (Martinis, 2017; Garg et al., 2024), confirming that coherence change detection is a reliable flood indicator in arid environments where intensity contrast is weak. A time series of coherence images, particularly the mean pre-flood coherence, provides a stable baseline for change detection and reduces random noise compared to single pre-flood coherence images.

4.3 Agricultural Environment (Hannover)

In Hannover, radar intensity decreased significantly in agricultural areas during the flood event, producing clearly distinguishable flooded areas. Coherence, however, showed only small variations and remained low before, during, and after the flood. This low and stable coherence is mainly caused by natural temporal decorrelation due to vegetation growth, soil moisture changes, and human activity, as noted by (Villarroya-Carpio and Lopez-Sanchez, 2023). As a result, coherence was not sensitive to short-term flooding, while intensity provided a much clearer signal.

For agricultural areas, intensity-based change detection using a pre-flood mean intensity image offers a reliable baseline and reduces noise. Coherence-based detection is less suitable because coherence changes rapidly and irregularly over time, which increases false alarms. In such cases, using a single pre-flood coherence image may be more appropriate for minimizing false detections.

Overall, the analysis shows that the performance of interferometric coherence and intensity for flood mapping strongly depends on the environmental setting.

5. Conclusion and Outlook

This research explored the potential and added value of interferometric coherence for flood mapping across three study areas with distinct surface characteristics using Sentinel-1 time series data. Rather than comparing coherence with SAR intensity, the study focused on understanding how coherence behaves before, during, and after flood events and to what extent it can enhance flood monitoring and mapping performance. The results reveal a clear environment-dependent behavior of Interferometric coherence. In the arid region of Sistan and Baluchestan, coherence exhibited a strong temporal decorrelation during flooding, clearly identifying visually inundated areas where intensity-based approaches struggled due to low backscatter in pre- and during flood events. In Hannover's agricultural environment, coherence remained lower value over time due to vegetation growth, soil moisture fluctuations, anthropogenic activities, and the sensitivity of SAR sensors, limiting its ability to detect low coherence values due to floods, whereas intensity continued to capture flood-related backscatter reductions. In the urban region of Valencia, coherence responses were moderate, with localized reductions around mixed surfaces such as the Turia river and its surroundings and agricultural areas, while built-up areas maintained high coherence.

Overall, this study demonstrates that interferometric coherence is a valuable but context-dependent complement to SAR intensity for flood mapping. Its greatest potential lies in arid regions, where intensity methods fail. Future research should focus on multi-temporal coherence metrics, utilizing adaptive coherence estimation rather than traditional boxcar coherence estimation. In addition, cross-sensor experiments such as L-band systems of NISAR satellite and hybrid frameworks combining coherence, intensity, and incorporating auxiliary data such as optical imagery could further improve flood mapping using Interferometric coherence.

6. Acknowledgement

This research was funded by the German Academic Exchange Service (DAAD). Sentinel-1 (2019-2024) and Sentinel-2A via Copernicus Hub; Landsat 8 OLI courtesy USGS.

References

Amitrano, D., Di Martino, G., Di Simone, A., Imperatore, P., 2024. Flood detection with SAR: A review of techniques and datasets. *Remote Sensing*, 16(4), 656.

Anusha, N., Bharathi, B., 2020. Flood detection and flood mapping using multi-temporal synthetic aperture radar and optical data. *The Egyptian Journal of Remote Sensing and Space Science*, 23(2), 207–219.

Bickel, D. L., 2014. Sar image effects on coherence and coherence estimation. Technical report, Sandia National Lab.(SNL-NM), Albuquerque, NM (United States).

Chini, M., Pelich, R., Li, Y., Hostache, R., Zhao, J., Di Mauro, C., Matgen, P., 2021. Sar-based flood mapping, where we are and future challenges. *2021 IEEE International Geoscience and Remote Sensing Symposium IGARSS*, IEEE, 884–886.

Delgado Blasco, J. M., Fitrzyk, M., Patruno, J., Ruiz-Armenteros, A. M., Marconcini, M., 2020. Effects on the double bounce detection in urban areas based on SAR polarimetric characteristics. *Remote Sensing*, 12(7), 1187.

DeVries, B., Huang, C., Armston, J., Huang, W., Jones, J. W., Lang, M. W., 2020. Rapid and robust monitoring of flood events using Sentinel-1 and Landsat data on the Google Earth Engine. *Remote sensing of Environment*, 240, 111664.

Ferretti, A., Fumagalli, A., Novali, F., Prati, C., Rocca, F., Rucci, A., 2011. A new algorithm for processing interferometric data-stacks: SqueeSAR. *IEEE transactions on geoscience and remote sensing*, 49(9), 3460–3470.

Fielding, E. J., Jung, J., 2024. Damage Proxy Mapping with SAR interferometric coherence change. *Procedia Computer Science*, 239, 2322–2328.

Frost, J., 2019. Introduction to statistics: An intuitive guide for analyzing data and unlocking discoveries. *(No Title)*.

Garg, S., Dasgupta, A., Motagh, M., Martinis, S., Selvakumaran, S., 2024. Unlocking the full potential of Sentinel-1 for flood detection in arid regions. *Remote Sensing of Environment*, 315, 114417.

Ishitsuka, K., Tsuji, T., Matsuoka, T., 2012. Detection and mapping of soil liquefaction in the 2011 Tohoku earthquake using SAR interferometry. *Earth, Planets and Space*, 64(12), 1267–1276.

Li, Y., Martinis, S., Wieland, M., Schlaffer, S., Natsuaki, R., 2019. Urban flood mapping using SAR intensity and interferometric coherence via Bayesian network fusion. *Remote Sensing*, 11(19), 2231.

Liao, H.-Y., Wen, T.-H., 2020. Extracting urban water bodies from high-resolution radar images: Measuring the urban surface morphology to control for radar’s double-bounce effect. *International journal of applied Earth observation and geoinformation*, 85, 102003.

Lu, C.-H., Ni, C.-F., Chang, C.-P., Yen, J.-Y., Chuang, R. Y., 2018. Coherence difference analysis of sentinel-1 SAR interferogram to identify earthquake-induced disasters in urban areas. *Remote Sensing*, 10(8), 1318.

Martinis, S., 2017. Improving flood mapping in arid areas using sentinel-1 time series data. *2017 IEEE international geoscience and remote sensing symposium (IGARSS)*, IEEE, 193–196.

Nico, G., Pappalepore, M., Pasquariello, G., Refice, A., Samarelli, S., 2000. Comparison of SAR amplitude vs. coherence flood detection methods-a GIS application. *International Journal of Remote Sensing*, 21(8), 1619–1631.

Oberstadler, R., Hönsch, H., Huth, D., 1997. Assessment of the mapping capabilities of ERS-1 SAR data for flood mapping: a case study in Germany. *Hydrological processes*, 11(10), 1415–1425.

Pandey, A. C., Kaushik, K., Parida, B. R., 2022. Google Earth Engine for large-scale flood mapping using SAR data and impact assessment on agriculture and population of Ganga-Brahmaputra basin. *Sustainability*, 14(7), 4210.

Papila, I., Alganci, U., Sertel, E., 2020. Sentinel-1 based flood mapping using interferometric coherence and intensity change detection approach. *The International Archives of the Photogrammetry, Remote Sensing and Spatial Information Sciences*, 43, 1697–1703.

Pulvirenti, L., Pierdicca, N., Chini, M., Guerriero, L., 2011. An algorithm for operational flood mapping from Synthetic Aperture Radar (SAR) data using fuzzy logic. *Natural Hazards and Earth System Sciences*, 11(2), 529–540.

Richards, J. A. et al., 2009. *Remote sensing with imaging radar*. 1, Springer.

Rosen, P. A., Hensley, S., Zebker, H. A., Webb, F. H., Fielding, E. J., 1996. Surface deformation and coherence measurements of Kilauea Volcano, Hawaii, from SIR-C radar interferometry. *Journal of Geophysical Research: Planets*, 101(E10), 23109–23125.

Sharifi, A., 2020. Flood mapping using relevance vector machine and SAR data: A case study from Aqqala, Iran. *Journal of the Indian Society of Remote Sensing*, 48(9), 1289–1296.

Soudagar, R., Bhardwaj, A., 2025. Urban Flood Extent Mapping by Integrating SAR Intensity and Coherence within a Gaussian Mixture Model Framework. *ISPRS Annals of the Photogrammetry, Remote Sensing and Spatial Information Sciences*, 847–853.

Stehman, S. V., 1999. Basic probability sampling designs for thematic map accuracy assessment. *International Journal of remote sensing*, 20(12), 2423–2441.

Touzi, R., Lopes, A., Bruniquel, J., Vachon, P. W., 2002. Coherence estimation for SAR imagery. *IEEE transactions on geoscience and remote sensing*, 37(1), 135–149.

Townsend, P. A., 2001. Mapping seasonal flooding in forested wetlands using multi-temporal Radarsat SAR. *Photogrammetric Engineering & Remote Sensing*, 67(7).

Twele, A., Cao, W., Plank, S., Martinis, S., 2016. Sentinel-1-based flood mapping: a fully automated processing chain. *International Journal of Remote Sensing*, 37(13), 2990–3004.

Vanama, V. S. K., Mandal, D., Rao, Y. S., 2020. GEE4FLOOD: rapid mapping of flood areas using temporal Sentinel-1 SAR images with Google Earth Engine cloud platform. *Journal of Applied Remote Sensing*, 14(3), 034505–034505.

Villarroya-Carpio, A., Lopez-Sanchez, J. M., 2023. Multi-annual evaluation of time series of Sentinel-1 interferometric coherence as a tool for crop monitoring. *Sensors*, 23(4), 1833.

Zebker, H., Villasenor, J. et al., 1992. Decorrelation in interferometric radar echoes. *IEEE Transactions on geoscience and remote sensing*, 30(5), 950–959.

Zhang, X., Chan, N. W., Pan, B., Ge, X., Yang, H., 2021. Mapping flood by the object-based method using backscattering coefficient and interference coherence of Sentinel-1 time series. *Science of the Total Environment*, 794, 148388.